

Patched Denoising Diffusion Models For High-Resolution Image Synthesis

Zheng Ding^{1*}, Mengqi Zhang^{1*}, Jiajun Wu², and Zhuowen Tu¹

¹University of California, San Diego

²Stanford University



Figure 1: Generated image of size 1024×512 using the model trained on 21k natural images using a 148M-parameters model.

Abstract

We propose an effective denoising diffusion model for generating high-resolution images (e.g., 1024×512), trained on small-size image patches (e.g., 64×64). We name our algorithm Patch-DM, in which a new feature collage strategy is designed to avoid the boundary artifact when synthesizing large-size images. Feature collage systematically crops and combines partial features of the neighboring patches to predict the features of a shifted image patch, allowing the seamless generation of the entire image due to the overlap in the patch feature space. Patch-DM produces high-quality image synthesis results on our newly collected dataset of nature images (1024×512), as well as on standard benchmarks of smaller sizes (256×256), including LSUN-Bedroom, LSUN-Church, and FFHQ. We compare our method with previous patch-based generation methods

and achieve state-of-the-art FID scores on all four datasets. Further, Patch-DM also reduces memory complexity compared to the classic diffusion models.

1. Introduction

Generative image modeling has a long history [14, 48, 9] in computer vision, and it has received major developments in multiple directions in the deep learning era [12].

We have seen explosive development in generative adversarial learning [44, 13, 31, 2, 19, 8], though many GAN models remain hard to train. VAE models [22] are easier to train, but the resulting image quality is often blurry. Diffusion generative models [40, 16, 42, 43, 5] have lately gained tremendous popularity with generated images of superb quality [32]. Despite the excellent modeling capability of generative diffusion models, the current models still face challenges in both training and synthesis.

*Equal Contribution.

Due to direct optimization in the pixel space and multi-timestep training and inference, diffusion models are hard to scale up to high-resolution image generation. Therefore, current state-of-the-art models either use super-resolution methods to increase the generated images to higher resolutions [32, 34], or optimize the latent space instead of the pixel space [33]. However, both types of approaches still consist of high-resolution image generators that consume a large memory with a big model size.

To ameliorate the limitations in the current diffusion models, we propose a new method, Patch-DM, to generate high-resolution images with a newly-introduced feature collage strategy. The basic operating point for Patch-DM is a patch-level model that is relatively compact compared to those modeling the entire image. Though it appears to have introduced compromises for a patch-based representation, Patch-DM can perform seamless full-size high-resolution image synthesis without artifacts of the boundary effects for pixels near the borders of the image patches. The effectiveness of Patch-DM in directly generating high-resolution images is enabled by a novel feature collage strategy. This strategy helps feature sharing by implementing a sliding-window based shifted image patch generation process, ensuring consistency across neighboring image patches; this is a key design in our proposed Patch-DM method to alleviate the boundary artifacts without requiring additional parameters. To summarize, the contributions of our work are listed as follows:

- We develop a new denoising diffusion model based on patches, Patch-DM, to generate images of high-resolutions. Patch-DM can perform direct high-resolution image synthesis without introducing boundary artifacts.
- We design a new feature collage strategy where each image patch to be synthesized obtains features partially from its shifted input patch. Through systematic window sliding, the entire image is being synthesized by forcing feature consistency across neighboring patches. This strategy, named feature collage, gives rise to a compact model of Patch-DM that is patch-based for high-resolution image generation.

Patch-DM points to a promising direction for generative diffusion modeling at a flexible patch-based representation level, which allows high-resolution image synthesis with lightweight models.

2. Related Work

Generative modeling. A basic design principle for generative modeling is to match empirical observations to the sample distribution based on image features pre-specified

by humans [14]. Statistically, the feature matching strategy can often be generalized under the minimal description length (MDL) principle [1, 6, 48]. In addition to MDL, a generative adversarial learning framework, named GDL [44], learns an energy-based generative model using adversarial training. In the deep learning era, three notable major developments have significantly enhanced the learning and modeling capability, namely generative adversarial neural networks (GAN) [13], variational auto-encoders [22], and diffusion models [40].

Generative diffusion models. Generative diffusion models [40, 16, 42] which learn to denoise noisy images into real images have gained much attention lately due to its training stability and high image quality. Lots of progress has been made in diffusion models such as faster sampling[41], conditional generation[28, 7] or high-resolution image synthesis[33]. The traits of diffusion models have been amplified particularly by the success of DALL-E 2 [32] and Imagen [34] which generate high quality images from the given texts.

Patch-based image synthesis. The practice of employing image patches of relatively small sizes to generate images of larger sizes has been a longstanding technique in computer vision and graphics, particularly in the context of exemplar-based texture synthesis [9]. While generative adversarial networks (GANs) have been utilized for expanding non-stationary textures [47], image synthesis is still considered more challenging due to the complex structures present in images. To address this challenge, COCO-GAN [24] uses micro coordinates and latent vectors to synthesize large images by generating small patches first. InfinityGAN [25] further improves this by introducing Structure Synthesizer and Padding Free Generator to disentangle global structures and local textures and also generate consistent pixel values at the same spatial locations. ALIS [39] proposes an alignment mechanism on latent and image space to generate larger images. Anyres-GAN [4], on the other hand, adopts a two-stage training method by first learning the global information from low-resolution downsampled images and then learning the detailed information from small patches.

Our work, Patch-DM consists of a new design, feature collage, in which partial features of neighboring patches are cropped and combined for predicting a shifted patch. We borrow the term “collage” from the picture collage task [46] for the ease of understanding of our method, though our feature collage strategy only has a loose conceptual connection to picture collage [46]. Adopting positional embedding in Patch-DM also makes it easier to maintain spatial regularity. Although Patch-DM employs a shifted window strategy, its motivation and implementation are different from those of the widely-known Swin Transformers [26].

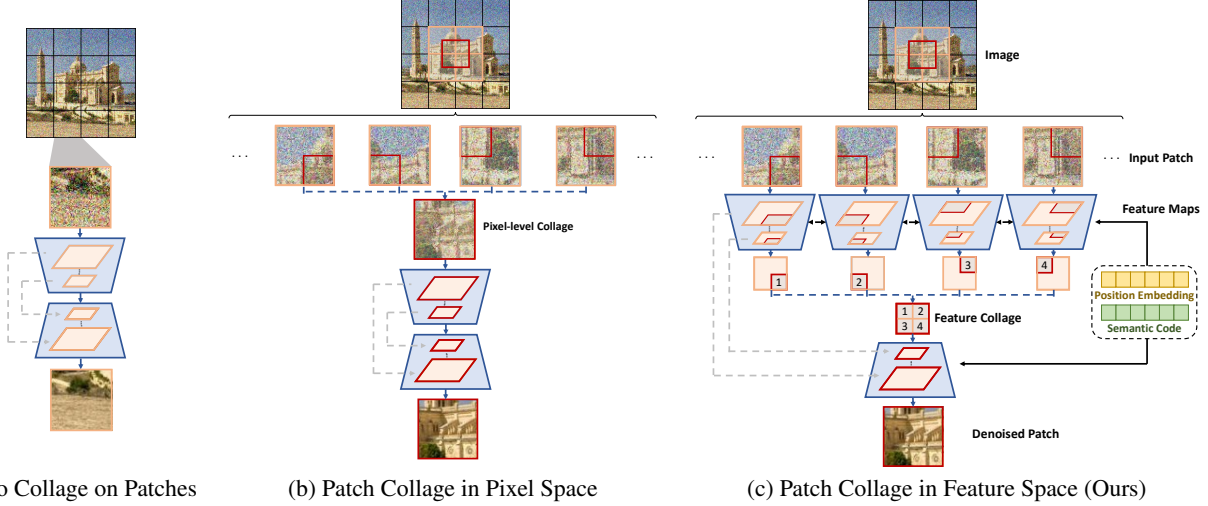


Figure 2: **Patch Generation For Image Synthesis.** (a) shows a very basic method of patch-wise image synthesis by simply splitting the images and generating patches independently. This method brings severe border artifacts. (b) alleviates the border artifacts by using shifted windows while generating images and doing patch collage in pixel space. (c) is our proposed method which collages the patches in the feature space. The features for neighboring features will be split and collaged for a new patch synthesis. We will show this method is a key design for us to generate high-quality images without border artifacts.

3. Background

Denoising diffusion models generate real images from randomly sampled noise images by learning a denoising function [16]. Instead of directly denoising the random noise image to a real image, denoising diffusion models learn to denoise the noise image through T steps. The forward process adds noise to the image x_0 gradually while the learned denoising function f_θ tries to reverse this process from the $x_T \sim \mathcal{N}(0, \mathbf{I})$. More formally, the forward process at time step $t (t = 1 \dots T)$ can be defined as

$$x_t \sim \mathcal{N}(x_{t-1}; \sqrt{1 - \beta_t}x_{t-1}, \beta_t \mathbf{I}), \quad (1)$$

where β_t are hyperparameters that control the noise, making the noise level of x_t gradually larger through the timesteps. Note that x_t can be directly derived from the original image x_0 since Eq. 1 can be rewritten as

$$x_t \sim \mathcal{N}(x_0; \sqrt{\alpha_t}x_0, (1 - \alpha_t)\mathbf{I}), \quad (2)$$

where $\alpha_t = \prod_{s=1}^t (1 - \beta_s)$. In order to generate the images from the noise input, the denoising model f_θ learns to reverse from x_t to x_{t-1} , which is defined as

$$\hat{\epsilon}_t = f_\theta(x_t, t), \quad (3)$$

$$x_{t-1} \sim \mathcal{N}(x_t; \frac{1}{\sqrt{1 - \beta_t}}(x_t - \frac{\beta_t}{\sqrt{1 - \alpha_t}}\hat{\epsilon}_t), \sigma_t \mathbf{I}), \quad (4)$$

where σ_t are hyperparameters that control the variance of the denoising process. The objective of the denoising model is $\|\epsilon_t - \hat{\epsilon}_t\|^2$. ϵ_t is ground truth noise added on image.

Therefore, after the denoising model is trained, the model can generate real images from random noise using Eq. 4. As can be seen, the whole generation process depends fully on the denoising process. Since the model denoises the image in the pixel space directly, the computation would be very expensive once the resolution gets higher.

4. Patched Denoising Diffusion Model

In this section, we describe our proposed Patched Denoising Diffusion Model (Patch-DM). Rather than using entire complete images for training, our model only takes patches for training and inference and uses feature collage to systematically combine partial features of neighboring patches. Consequently, Patch-DM is capable of resolving the issue of high computational costs associated with generating high-resolution images, as it is resolution-agnostic.

Before we dive into our model's training details, we first give an overview of the image generation process of our method. The training image from the dataset is $x_0 \in \mathbf{R}^{C \times H \times W}$, we split x_0 into $x_0^{(i,j)}$ where i, j is the row and column number of the patch, $x_0^{(i,j)} \in \mathbf{R}^{C \times h \times w}$. Instead of directly generating x_0 like most of methods do, our model only generates $x_0^{(i,j)}$ and concatenate them together to form a complete image.

A very basic way to do this is what we show in Figure 2(a) where the denoising model takes the noised image patch $x_t^{(i,j)}$ as input and output the corresponding noise $\hat{\epsilon}_t^{(i,j)}$. However, since the patches do not interact with each other, there will be severe borderline artifacts.

A further way to do this is to shift image patches during each time step depicted in Figure 2(b). At different time steps, the model will take either the original split patch $x_t^{(i,j)}$ or the shifted split patch $x_t^{\prime(i,j)}$ so that the border artifacts can be alleviated which we call ‘‘Patch Collage in Pixel Space’’. However, in Section 6 we show that the border artifacts still exist.

To further improve this method, we propose a novel feature collage mechanism depicted in Figure 2(c). Instead of performing patch collage in the pixel space, we perform it in the feature space. This allows the patches to be more cognizant of the adjacent features and prevent border artifacts from appearing while generating the complete images. More formally,

$$[z_1^{(i,j)}, z_2^{(i,j)}, \dots, z_n^{(i,j)}] = f_\theta^E(x_t^{(i,j)}, t), \quad (5)$$

where f_θ^E is the UNet encoder and $z_1^{(i,j)}, z_2^{(i,j)}, \dots, z_n^{(i,j)}$ are the internal feature maps. We then split the feature maps and collage the split feature maps to generate shift patches

$$\hat{z}_k^{(i,j)} = [P_1(z_k^{(i,j)}), P_2(z_k^{(i,j+1)}), P_3(z_k^{(i+1,j)}), P_4(z_k^{(i+1,j+1)})], \quad (6)$$

where P_1, P_2, P_3, P_4 are split functions as shown in Figure 2(c). Then we send these collaged shift features $\hat{z}_k^{(i,j)}$ to the UNet decoder to get the predicted shift patch noise:

$$\epsilon_t^{\prime(i,j)} = f_\theta^D([z_1^{\prime(i,j)}, z_2^{\prime(i,j)}, \dots, z_n^{\prime(i,j)}], t). \quad (7)$$

In order to make the model generate more semantically consistent images, we also add position embedding and semantic embedding to the model so that f_θ will take another two inputs which are $\mathcal{P}(i, j)$ and $\mathcal{E}(x_0)$.

During inference time, we take a 3x3 example as illustrated in Figure 3, in order to generate the border patches, we first pad the images so that the feature collage can be done for each patch without information loss. At each time step t , image x_t is decomposed into patches which are fed into the subsequent encoder. Before a feature map goes through the decoder, a split and collage operation is applied to it. Thus, the decoder outputs the predicted noise of the shifted patch. According to Eq. 4, we are able to obtain x_{t-1} and thus generate the final complete images.

5. Experiments

5.1. Implementation Details

Architecture. For the model architecture, we base our denoising U-Net model from [7] with changes of taking global conditions and positional embeddings. We use two methods to obtain the global conditions. The first is to use a pretrained model to obtain the image features and use the

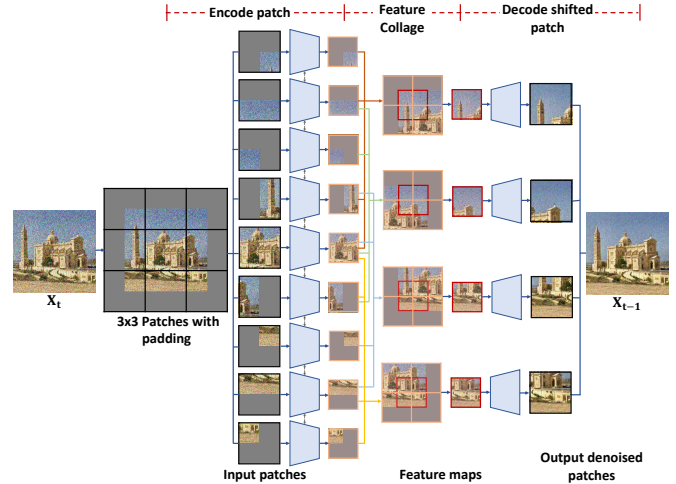


Figure 3: **Detailed Inference process at each time step.** For simplicity, 256×256 images and 3×3 patch decomposition is used for illustration. The image is padded and patchified. The patches then go through the encoder independently. Four adjacent obtained feature maps after encoding are concatenated, and a new patch in the middle with red borders is extracted. The newly obtained patches can be viewed as results of the shift window operated on the feature level. The decoder is to predict the noise level inside each shifted patch. The final denoised image x_{t-1} can then be obtained.

image features as the global conditions, while optimizing the features directly during training. In this case, we do not have to increase the model parameters and can scale to high-resolution images. However, when the number of images in the training dataset is too large, optimizing the pre-obtained image features requires more effort. We use this approach for global conditioning when training on datasets of 1024×512 images. The pretrained model we use for obtaining the image embeddings is CLIP [30]. We resize the images to 224×224 and send them to ViT-B/16 to obtain the features as global conditions; we then optimize these global conditions directly.

The second is jointly training an image encoder and using its output as the global conditions. Here, the jointly training image encoder may borrow the same architecture as in the denoising U-Net’s encoder. It works particularly well when the training dataset is large. However, it requires another model, which would be a bottleneck in training on high-resolution datasets, since the computation would increase significantly as the resolution increases. We use this approach when training on large datasets of 256×256 images. We utilize global conditions with a dimension of 512 in both methods.

Classifier-free guidance. We also use the classifier-free guidance [17] to improve the training speed and quality. We use classifier-free guidance on both the global conditions and position embeddings. The dropout rate is 0.1 for the global conditions and 0.5 for position embeddings.

Method	Patch Size	FID ↓	sFID ↓	IS ↑	Precision ↑	Recall ↑
COCO-GAN [24]	64×64	70.980	74.208	4.744	0.2062	0.0832
InfinityGAN [25]	101×101	46.550	70.041	5.736	0.3156	0.2603
Anyres-GAN [4]	64×64	44.173	34.430	4.357	0.3649	0.1190
Patch-DM (Ours)	64×64	20.369	34.405	5.604	0.6765	0.2644

Table 1: Quantitative comparison with previous patch-based image generation methods. All models are trained on the natural images dataset (1024×512). We use FID to measure the overall quality of generated images and sFID for the quality of high-level structures. In addition, we use IS (Inception Score) and Precision to measure sample fidelity and Recall for diversity.



Figure 4: Generated 2048×1024 image. We double the number of patches so that the model can generate images with 2x resolution from 1024×512. The left image is a 2048×1024 image, and the right image is a zoom-in of the red bounding box, with a resolution of 256×256.

Patch size. We use a patch size of 64×64 in all our experiments. The denoising U-Net model’s architecture is the same across all the datasets, as it is only related to the patch size regardless of the training images’ resolution.

Inference. Once the denoising U-Net model has been trained, we train another latent diffusion model for unconditional image synthesis. The latent diffusion model’s architecture is based on the one described in [29]. The data we use for training the latent diffusion model is either from the output of the trained image encoder or the directly optimized image embeddings. To synthesize an image, we will first sample a latent code from the latent diffusion model and then use this latent code to serve as the global conditions for sampling an image. During the sampling stage, we use the inference process proposed by DDIM [41] and set the sampling step to 50.

Evaluation. We conduct both qualitative and quantitative evaluations on four datasets. For quantitative evaluation, we use FID, a popular metric in generative modeling [15]. Additionally, we also provide results on sFID [27], Inception Score [36], Improved Precision and Recall [23]. To compute FID, we follow the setting of [15] and generate 50K images to compute the metrics over the full dataset. We apply the same setting for sFID and Inception Score computation. For Improved Precision and Recall, we use the same generated 50K over 10K images randomly chosen from the dataset following the setting of [7].

5.2. Results on 1024×512 Images

Setup. To show our model’s capability on direct high-resolution image synthesis, we collect 21443 natural images from [45]. The resolution we use is 1024×512. We split each image into 16×8 patches; therefore, a single patch has the size of 64×64.

We use the CLIP ViT-B/16 pretrained image visual encoder to obtain the image embeddings first. While down-sampling to fit the CLIP model may result in the loss of some detailed image information in the embeddings, these details can still be ”recovered” during the embedding optimization in the training process, aided by the supervision of the original high-resolution image. Each image patch can be trained and sampled independently with feature collage assisting to be aware of the surrounding information. Since every image is segmented into smaller patches, the total number of model parameters is much smaller than other large diffusion models.

As most existing diffusion models merely can directly generate images of 1k resolution, and the general strategy for high-resolution synthesis is to sample hierarchically (generate relatively low-resolution images first and then perform super-resolution), our Patch-DM simplifies sample procedure using much more lightweight models, which is one of the main advantages.

Results. We compare our model with previous patch-based image generation methods in Table 1. From the table, we



Figure 5: Generated images on FFHQ, LSUN-Bedroom, and LSUN-Church datasets. All the resolutions are 256×256 .

can see our method delivers the best overall quality of the generated images. Our method also outperforms previous patch-based generation models on sFID, Precision and Recall with only IS a little bit worse than InfinityGAN. Apart from the quantitative evaluation, we also present an image generated by our model in Figure 1. For more generated images, please refer to our supplementary materials.

5.3. Results on 256×256 Images

Setup. To compare with other existing generative models, we also train our Patch-DM on three standard public datasets: FFHQ, LSUN-Bedroom, and LSUN-Church, and evaluate its sampling performance. All the resolution is 256×256 . Thus, the number of patches is 4×4 . Notice that the model architecture keeps the same; the only change here is the number of patches during training and inference. We use the same training setting across the three datasets.

Results. We report the quantitative results in Table 2 and qualitative results in Figure 5, respectively. In Table 2, we can see our model achieves competitive results while still outperforms previous patch-based methods. Figure 5 illustrates that despite producing small image patches, our denoising model exhibits minimal boundary artifacts and offers good visual quality. This demonstrates the effectiveness of our feature collage mechanism.

Model size comparison. Compared with other widely used diffusion models, our proposed method could achieve competitive performance using a smaller model with above mentioned indispensable components. Patch-DM is fully built upon the network on 64×64 patches regardless of the target image resolution and uses optimized global conditions to avoid the increase of model parameter amounts brought by higher input resolution. Comparison of model parameters with other classic diffusion models on 256×256 resolution is shown in Table 3. Notice that we use the same model for the 512×1024 resolution except the semantic embedding method as previously present.

FFHQ 256×256					
Method	FID ↓	sFID ↓	IS ↑	Prec. ↑	Recall ↑
DiffAE (s = 50) [29]	9.71	10.24	4.60	0.71	0.45
LDM-4 (s = 50) [33]	8.76	7.09	4.54	0.66	0.45
UDM [20]	5.54	-	-	-	-
U-Net GAN + aug [38]	7.48	-	4.46	-	-
BigGAN [3]	11.48	-	3.97	-	-
Taming Transformer [11]	9.60	16.58	3.99	0.70	0.37
ProjectedGAN [37]	3.08	-	-	0.65	0.46
COCO-GAN[24]					
InfinityGAN [25]	34.02	37.44	3.92	0.36	0.08
Anyres-GAN [4]	28.87	127.92	4.02	0.40	0.16
Patch-DM (Ours, s = 50)	24.48	55.77	3.38	0.67	0.25
LSUN-Bedroom 256×256					
Method	FID ↓	sFID ↓	IS ↑	Prec. ↑	Recall ↑
ADM (s = 1000) [7]	1.90	5.59	2.38	0.66	0.51
LDM-4 (s = 50) [33]	3.40	7.53	2.27	0.60	0.49
UDM [20]	4.57	-	-	-	-
IDDPM [28]	4.24	8.21	2.36	0.62	0.46
PGGAN [18]	8.34	9.21	2.50	0.48	0.40
StyleGAN [19]	2.35	6.62	2.55	0.59	0.48
COCO-GAN[24]					
InfinityGAN [25]	41.84	62.69	2.63	0.18	0.14
Anyres-GAN [4]	10.71	19.28	2.17	0.43	0.35
Patch-DM (Ours, s = 50)	15.65	56.24	1.79	0.69	0.14
LSUN-Church 256×256					
Method	FID ↓	sFID ↓	IS ↑	Prec. ↑	Recall ↑
LDM-8 (s = 50) [33]	4.23	11.44	2.69	0.71	0.50
DDPM [16]	7.89	-	-	-	-
PGGAN [18]	6.42	10.48	2.56	0.65	0.39
StyleGAN [19]	4.21	-	-	-	-
ImageBART [10]	7.32	-	-	-	-
COCO-GAN[24]					
InfinityGAN [25]	17.91	73.94	2.66	0.47	0.16
Anyres-GAN [4]	7.08	33.58	2.56	0.60	0.36
Patch-DM (Ours, s = 50)	17.09	80.66	2.10	0.65	0.17
COCO-GAN[24]					
InfinityGAN [25]	5.49	14.80	2.85	0.62	0.53

Table 2: Evaluation Metrics of unconditional image synthesis on three 256×256 datasets: FFHQ, LSUN-Bedroom, and LSUN-Church. $s = N$ refers to sampling steps in diffusion models. For a fair comparison, results are reproduced in the same sampling steps as ours, using provided pretrained checkpoints of other diffusion models. We adopt a patch size of 64×64 for Patch-DM, Anyres-GAN, COCO-GAN and 101×101 for InfinityGAN. We bold and underline the numbers to denote the best numbers across all methods. Numbers only bolded denote the best numbers in the same category.

Method	Model Size ↓
Base model + Super-resolution	
SR3 [35]	B[64]+625M
Direct generation	
ADM [21]	552M
DiffAE [29]	232M
LDM-4 [33]	274M
Patch-DM (Ours, full model)	154M
Patch-DM (Ours, w/ SE, w/o latent DPM)	91M
Patch-DM (Ours, w/o SE, w/o latent DPM)	70M

Table 3: Number of parameters comparison between different diffusion models on 256×256 resolution. SE means semantic encoder to extract global information. The size of our previously trained 1024×512 model is $70M + [\text{size of optimized semantic embeddings}]$ during training and $[63M \text{ latent DPM}]$ in inference.

5.4. Applications

We now demonstrate four applications of our Patch-DM. All of them are conducted without post-training.

Beyond patch generation. Since our method samples images using patches, during testing, we have the option to incorporate more patches during testing. This enables the model to produce images with higher resolutions compared to the ones in the training set without requiring further training. We adopt two ways to achieve this.

The first one is to add patches inside the original images so that the generated images can have a $2 \times$ resolution compared to the ones in the training dataset. We experiment this on our collected 21K natural images. We insert patches inside all the existing ones, thus making the patch number increase from 16×8 to 32×16 . The global conditions we use for these patches is the same as the original, while we interpolate the position embeddings in this setting to see how the network could learn from the unseen position embeddings. We provide a generated 2048×1024 image in Figure 4. As can be seen, our model can still generate consistent patches even though the newly added patches have never been used in the training process.

The second one is to add patches outside the original image. This way is similar to beyond-boundary generation in COCO-GAN[24] with a key difference that it needs a post-training process to improve the continuity among patches. We conduct an experiment on LSUN-Bedroom and LSUN-Church by adding more patches. The original resolution in the training data we use is 256×256 , which is divided by 4×4 patches. We add more patches to the existing 4×4 patches so that the number grows to 6×6 . Therefore, the model can generate an image with a resolution of 384×384 . For the original 4×4 patches, we use the condition generated from the latent diffusion model and the position embeddings as pre-defined. For the additional patches, we use the same semantic condition, while we don't use position embeddings for these added ones. Thus the model needs to synthesize the additional patches only according to the global conditions and the neighboring context information. We present our results in Figure 6 and

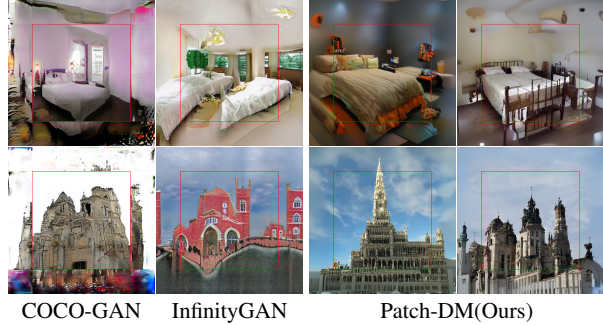


Figure 6: **Synthesized 384×384 images on LSUN-Bedroom (256×256) and LSUN-Church (256×256).** Despite only being trained on 256×256 images, our model can generate 384×384 images by adding more patches (outside the red bounding box). Extended images generated by our models are compared with COCO-GAN and InfinityGAN, which also have the ability to extend fields without further training.



Figure 7: **Image outpainting on LSUN-Church and LSUN-Bedroom.** The image inside the red bounding box is the input image from the validation dataset. We pad the image patches from 4×4 to 6×6 to enable the image outpainting. The image parts outside the red bounding box are the outpainting results.

compare it with COCO-GAN[24] without post-training and InfinityGAN[25] under the same setting.

Image outpainting. Another practical application would be image outpainting that only draws the outer part of the image while keeping the input image the same. To do this, we experiment using the model trained on LSUN-Church and LSUN-Bedroom. First, we send images from the LSUN-Church validation dataset and LSUN-Bedroom validation dataset to the image encoder to obtain the global conditions. Then, to keep the original image the same, we replace the inner predicted noised image patches with the ground truth noised images patches (adding corresponding noise to the input images) during each timestep while sampling. We present our results in Figure 7. It can be seen from the results that our model can “imagine” the surrounding areas reasonably and generate rather consistent outer parts of the image without obvious border effects.

Image inpainting. In this task, we infill the corrupted images with random masks, which requires the restored results to be consistent in context. We experiment on the LSUN-Church validation set using already trained models without further tailored training. The original images are masked by different numbers of blocks ranging from 1 to 6, and the sampling process is only conditioned on local position embeddings w/o global conditions. The results are presented



Figure 8: **Image Inpainting on LSUN-Church.** Each row has two pairs of corrupted and restored images. For each pair, the left side is the masked image; the right one is the inpainted result by our model without further training on this task. The mask number, i.e., the number of patches the model needs to repair, is increasing from left to right and from top to bottom.

in Figure 8. From the figure, we can see that our model can infill the blocks consistently using surrounding patches, demonstrating that feature collage facilitates the model with the capability to be aware of adjacent information, enabling it to be naturally applied to inpainting tasks.

6. Ablation Study

Three indispensable components: semantic code, position embeddings and shift window strategy on feature levels, considerably eliminate border artifacts and improve our model performance. Here, we conduct ablation study to investigate the effects of these modules. We provide both qualitative results and quantitative results in Figure 9 and Table 4 respectively.

Global conditions. We study the problem without global conditions; thus, the generation process will fully rely on the positional embedding and neighboring context information. We present our images in Figure 9 (a). It’s interesting to see how the model generates when no global conditions are given, which is a strong constraint for the model to generate semantic-related patches. From the given image, we can see that the model can still generate locally-consistent images; the image quality is however relatively low.

Position embeddings. The last section shows that global conditions are necessary for our model to generate high-quality images. We then condition the model only on those to investigate the role of positional embeddings. The results are shown in Figure 9 (b). Without the position information, the model would generate distorted images with patchTheelonging to where they should be, although the whole image may follow a certain style. Hence, the positional embeddings are vital to our model.

Collage in the pixel space. A straightforward idea is to perform collage in the pixel space as present in Figure 2(b); the images are decomposed by window-shifted



Figure 9: Ablation study on the effect of global conditions (a), position embeddings (b), and feature level shift (c, d).

Method	FID (1k) ↓
No global semantic condition	79.33
No position embedding	48.82
Pixel space fixed shift	49.80
Pixel space random shift	52.11
Patch-DM (Ours)	37.99

Table 4: FID evaluation on 1,000 images of different ablation settings to investigate the importance of semantic condition, position embedding, and feature-level window shift.

patches from their original positions. To maintain patch size consistency, we add zero padding around the image. For the sampling procedure: In an odd-number step, original patches are generated independently, while in an even-number step, patches with shifted positions are sampled.

Under this scheme, we experiment in two different settings. The first is to take a fixed shift step (half patch size) along the height and width direction. The sample result is shown in Figure 9(c). There are still apparent artifacts along the border. This proves that even though the shift window on the image level could enable patches to be aware of surroundings during sampling, the awareness level is quite limited, and the final generation is similar to breaking the image into smaller patches.

The second setting is to shift the patch position with a randomly sampled step ranging from zero to patch size. The inference result is shown in Figure 9(d). The sample quality is much improved compared to the previous situation. However, the result is still not as photo-realistic as Patch-DM. The reason is that although the random shift enables finer surrounding awareness, it lacks in-depth feature interaction as our model does. Therefore, the feature-level window shift and collage can significantly eliminate border artifacts and improve final inference quality.

7. Conclusion

We have presented a new algorithm, Patch-DM, a patch-based denoising diffusion model for generating high-resolution images. We introduce a feature collage strategy to combat the boundary effect for patch-based image synthesis. Patch-DM achieves a significant reduction in model size and training complexity compared to the standard diffusion models trained on the original size images. Competitive quantitative and qualitative results are obtained for Patch-DM when trained on several image datasets.

Acknowledgement This work is supported by NSF Award IIS-2127544.

References

- [1] David H Ackley, Geoffrey E Hinton, and Terrence J Sejnowski. A learning algorithm for boltzmann machines. *Cognitive science*, 9(1):147–169, 1985. **2**
- [2] Martin Arjovsky, Soumith Chintala, and Léon Bottou. Wasserstein generative adversarial networks. In *ICML*, 2017. **1**
- [3] Andrew Brock, Jeff Donahue, and Karen Simonyan. Large scale gan training for high fidelity natural image synthesis. *arXiv preprint arXiv:1809.11096*, 2018. **6**
- [4] Lucy Chai, Michael Gharbi, Eli Shechtman, Phillip Isola, and Richard Zhang. Any-resolution training for high-resolution image synthesis. In *Computer Vision–ECCV 2022: 17th European Conference, Tel Aviv, Israel, October 23–27, 2022, Proceedings, Part XVI*, pages 170–188. Springer, 2022. **2, 5, 6**
- [5] Florinel-Alin Croitoru, Vlad Hondru, Radu Tudor Ionescu, and Mubarak Shah. Diffusion models in vision: A survey. *arXiv preprint arXiv:2209.04747*, 2022. **1**
- [6] Stephen Della Pietra, Vincent Della Pietra, and John Lafferty. Inducing features of random fields. *IEEE transactions on pattern analysis and machine intelligence*, 19(4):380–393, 1997. **2**
- [7] Prafulla Dhariwal and Alexander Nichol. Diffusion models beat gans on image synthesis. *Advances in Neural Information Processing Systems*, 34:8780–8794, 2021. **2, 4, 5, 6, A1**
- [8] Jeff Donahue, Philipp Krähenbühl, and Trevor Darrell. Adversarial feature learning. In *ICLR*, 2017. **1**
- [9] Alexei A Efros and Thomas K Leung. Texture synthesis by non-parametric sampling. In *Proceedings of the seventh IEEE international conference on computer vision*, pages 1033–1038, 1999. **1, 2**
- [10] Patrick Esser, Robin Rombach, Andreas Blattmann, and Bjorn Ommer. Imagebart: Bidirectional context with multinomial diffusion for autoregressive image synthesis. *Advances in Neural Information Processing Systems*, 34:3518–3532, 2021. **6**
- [11] Patrick Esser, Robin Rombach, and Bjorn Ommer. Taming transformers for high-resolution image synthesis. In *Proceedings of the IEEE/CVF conference on computer vision and pattern recognition*, pages 12873–12883, 2021. **6**
- [12] Ian Goodfellow, Yoshua Bengio, and Aaron Courville. *Deep learning*, volume 1. MIT Press, 2016. **1**
- [13] Ian Goodfellow, Jean Pouget-Abadie, Mehdi Mirza, Bing Xu, David Warde-Farley, Sherjil Ozair, Aaron Courville, and Yoshua Bengio. Generative adversarial nets. In *Advances in neural information processing systems*, 2014. **1, 2**
- [14] David J Heeger and James R Bergen. Pyramid-based texture analysis/synthesis. In *SIGGRAPH*, pages 229–238, 1995. **1, 2**
- [15] Martin Heusel, Hubert Ramsauer, Thomas Unterthiner, Bernhard Nessler, and Sepp Hochreiter. Gans trained by a two time-scale update rule converge to a local nash equilibrium. *Advances in neural information processing systems*, 30, 2017. **5**
- [16] Jonathan Ho, Ajay Jain, and Pieter Abbeel. Denoising diffusion probabilistic models. *Advances in Neural Information Processing Systems*, 33:6840–6851, 2020. **1, 2, 3, 6**
- [17] Jonathan Ho and Tim Salimans. Classifier-free diffusion guidance. *arXiv preprint arXiv:2207.12598*, 2022. **4**
- [18] Tero Karras, Timo Aila, Samuli Laine, and Jaakko Lehtinen. Progressive growing of gans for improved quality, stability, and variation. *arXiv preprint arXiv:1710.10196*, 2017. **6**
- [19] Tero Karras, Samuli Laine, and Timo Aila. A style-based generator architecture for generative adversarial networks. In *Proceedings of the IEEE conference on computer vision and pattern recognition*, pages 4401–4410, 2019. **1, 6**
- [20] Dongjun Kim, Seungjae Shin, Kyungwoo Song, Wanmo Kang, and Il-Chul Moon. Soft truncation: A universal training technique of score-based diffusion model for high precision score estimation. In *International Conference on Machine Learning*, pages 11201–11228. PMLR, 2022. **6**
- [21] Durk P Kingma and Prafulla Dhariwal. Glow: Generative flow with invertible 1x1 convolutions. In *Advances in Neural Information Processing Systems*, 2018. **7**
- [22] Diederik P Kingma and Max Welling. Auto-encoding variational bayes. In *ICLR*, 2014. **1, 2**
- [23] Tuomas Kynkäänniemi, Tero Karras, Samuli Laine, Jaakko Lehtinen, and Timo Aila. Improved precision and recall metric for assessing generative models. *Advances in Neural Information Processing Systems*, 32, 2019. **5**
- [24] Chieh Hubert Lin, Chia-Che Chang, Yu-Sheng Chen, Da-Cheng Juan, Wei Wei, and Hwann-Tzong Chen. Coco-gan: generation by parts via conditional coordinating. In *ICCV*, pages 4512–4521, 2019. **2, 5, 6, 7**
- [25] Chieh Hubert Lin, Yen-Chi Cheng, Hsin-Ying Lee, Sergey Tulyakov, and Ming-Hsuan Yang. InfinityGAN: Towards infinite-pixel image synthesis. In *ICLR*, 2022. **2, 5, 6, 7**
- [26] Ze Liu, Yutong Lin, Yue Cao, Han Hu, Yixuan Wei, Zheng Zhang, Stephen Lin, and Baining Guo. Swin transformer: Hierarchical vision transformer using shifted windows. In *Proceedings of the IEEE/CVF International Conference on Computer Vision*, 2021. **2**
- [27] Charlie Nash, Jacob Menick, Sander Dieleman, and Peter W Battaglia. Generating images with sparse representations. *arXiv preprint arXiv:2103.03841*, 2021. **5**
- [28] Alexander Quinn Nichol and Prafulla Dhariwal. Improved denoising diffusion probabilistic models. In *International Conference on Machine Learning*, pages 8162–8171. PMLR, 2021. **2, 6**
- [29] Konpat Preechakul, Nattanat Chatthee, Suttisak Wizadwongsa, and Supasorn Suwajanakorn. Diffusion autoencoders: Toward a meaningful and decodable representation. In *Proceedings of the IEEE/CVF Conference on Computer Vision and Pattern Recognition*, pages 10619–10629, 2022. **5, 6, 7, A1**
- [30] Alec Radford, Jong Wook Kim, Chris Hallacy, Aditya Ramesh, Gabriel Goh, Sandhini Agarwal, Girish Sastry, Amanda Askell, Pamela Mishkin, Jack Clark, et al. Learning transferable visual models from natural language supervision. In *International Conference on Machine Learning*, pages 8748–8763. PMLR, 2021. **4**

- [31] Alec Radford, Luke Metz, and Soumith Chintala. Unsupervised representation learning with deep convolutional generative adversarial networks. In *ICLR*, 2016. 1
- [32] Aditya Ramesh, Prafulla Dhariwal, Alex Nichol, Casey Chu, and Mark Chen. Hierarchical text-conditional image generation with clip latents. *arXiv preprint arXiv:2204.06125*, 2022. 1, 2
- [33] Robin Rombach, Andreas Blattmann, Dominik Lorenz, Patrick Esser, and Björn Ommer. High-resolution image synthesis with latent diffusion models. In *Proceedings of the IEEE/CVF Conference on Computer Vision and Pattern Recognition*, pages 10684–10695, 2022. 2, 6, 7
- [34] Chitwan Saharia, William Chan, Saurabh Saxena, Lala Li, Jay Whang, Emily Denton, Seyed Kamyar Seyed Ghasemipour, Burcu Karagol Ayan, S Sara Mahdavi, Rapha Gontijo Lopes, et al. Photorealistic text-to-image diffusion models with deep language understanding. *arXiv preprint arXiv:2205.11487*, 2022. 2
- [35] Chitwan Saharia, Jonathan Ho, William Chan, Tim Salimans, David J Fleet, and Mohammad Norouzi. Image super-resolution via iterative refinement. In *ICLR Workshop Track*, 2022. 7
- [36] Tim Salimans, Ian Goodfellow, Wojciech Zaremba, Vicki Cheung, Alec Radford, and Xi Chen. Improved techniques for training gans. In *Advances in Neural Information Processing Systems*, 2016. 5
- [37] Axel Sauer, Kashyap Chitta, Jens Müller, and Andreas Geiger. Projected gans converge faster. *Advances in Neural Information Processing Systems*, 34:17480–17492, 2021. 6
- [38] Edgar Schonfeld, Bernt Schiele, and Anna Khoreva. A unet based discriminator for generative adversarial networks. In *Proceedings of the IEEE/CVF conference on computer vision and pattern recognition*, pages 8207–8216, 2020. 6
- [39] Ivan Skorokhodov, Grigorii Sotnikov, and Mohamed Elhoseiny. Aligning latent and image spaces to connect the unconnectable. In *Proceedings of the IEEE/CVF International Conference on Computer Vision*, pages 14144–14153, 2021. 2
- [40] Jascha Sohl-Dickstein, Eric Weiss, Niru Maheswaranathan, and Surya Ganguli. Deep unsupervised learning using nonequilibrium thermodynamics. In *International Conference on Machine Learning*, pages 2256–2265, 2015. 1, 2
- [41] Jiaming Song, Chenlin Meng, and Stefano Ermon. Denoising diffusion implicit models. *arXiv preprint arXiv:2010.02502*, 2020. 2, 5
- [42] Yang Song and Stefano Ermon. Improved techniques for training score-based generative models. *Advances in neural information processing systems*, 33:12438–12448, 2020. 1, 2
- [43] Yang Song, Jascha Sohl-Dickstein, Diederik P Kingma, Abhishek Kumar, Stefano Ermon, and Ben Poole. Score-based generative modeling through stochastic differential equations. In *International Conference on Learning Representations*, 2020. 1
- [44] Zhuowen Tu. Learning generative models via discriminative approaches. In *CVPR*, 2007. 1, 2
- [45] Wallpaperscraft. Wallpaperscraft. <https://wallpaperscraft.com/>. 5
- [46] Jingdong Wang, Long Quan, Jian Sun, Xiaoou Tang, and Heung-Yeung Shum. Picture collage. In *CVPR*, pages 347–354, 2006. 2
- [47] Yang Zhou, Zhen Zhu, Xiang Bai, Dani Lischinski, Daniel Cohen-Or, and Hui Huang. Non-stationary texture synthesis by adversarial expansion. *ACM Transactions on Graphics (TOG)*, 37(4):1–13, 2018. 2
- [48] Song Chun Zhu, Ying Nian Wu, and David Mumford. Minimax entropy principle and its application to texture modeling. *Neural Computation*, 9(8):1627–1660, 1997. 1, 2

Appendix

A. Model Hyperparameters

For model architecture, we base our diffusion model from [7] with changes of taking global semantic condition and positional embedding. The hyperparameters for the main denoising U-Net model are specified in Table 5. Since the model is resolution agnostic, the main architectures for all datasets keep the same. We adopt two methods to obtain global semantic conditions: for relatively low-resolution images, an encoder is trained with architecture borrowed from the first half of the U-Net model, and the architecture details of the encoder are shown in Table 6. For high-resolution images such as 1024×512 , a pretrained image encoder is used to avoid scaling up the overall model size. We use ViT-B/16 in CLIP to obtain the image embeddings and optimize them during training. For position embeddings, we use sinusoidal positional embeddings. Time embedding and positional embedding are concatenated and modulated into ResBlocks together with the global code.

For realizing unconditional image synthesis, a latent diffusion model is trained on semantic embeddings. The implementation is based on the one proposed in [29] with MLP + skip connections architecture. The parameter details are specified in Table 7.

B. More Qualitative Results

We provide more unconditional sampling results with the models trained on our self-collected nature images (1024×512) in Figure 10-12 as well as three other standard benchmarks with a resolution of 256×256 : LSUN-Bedroom (Figure 13), LSUN-Church (Figure 14), and FFHQ (Figure 15). Additionally, we train our model on high-resolution FFHQ (1024×1024) dataset and provide the results in Figure 16.

Parameter	Patch-DM
Patch input size	$3 \times 64 \times 64$
Channel multiplier	[1, 2, 4, 8]
Net channel	64
ResBlock number	2
Attention resolution	16
Batch size	16
Diffusion steps	1000
Noise scheduler	Linear
Learning rate	0.0001
Optimizer	Adam

Table 5: Model Architecture for diffusion model.

Parameter	Semantic Encoder
Input size	$3 \times 256 \times 256$
Channel multiplier	[1, 2, 4, 8, 8]
Net channel	64
ResBlock number	2
Attention resolution	16
Global condition dimension	512
Batch size	16
Learning rate	0.0001
Optimizer	Adam

Table 6: Model Architecture for image semantic encoder.

Parameter	Latent Diffusion
Input size	512
MLP layers	10
MLP hidden size	2048
Noise scheduler	Constant 0.008
Batch size	256
Learning rate	0.0001
Optimizer	Adam (weight decay 0.01)

Table 7: Model Architecture for latent diffusion model.



Figure 10: Additional qualitative results on self-collected nature dataset (1024×512).



Figure 11: Additional qualitative results on self-collected nature dataset (1024×512).



Figure 12: Additional qualitative results on self-collected nature dataset (1024×512).

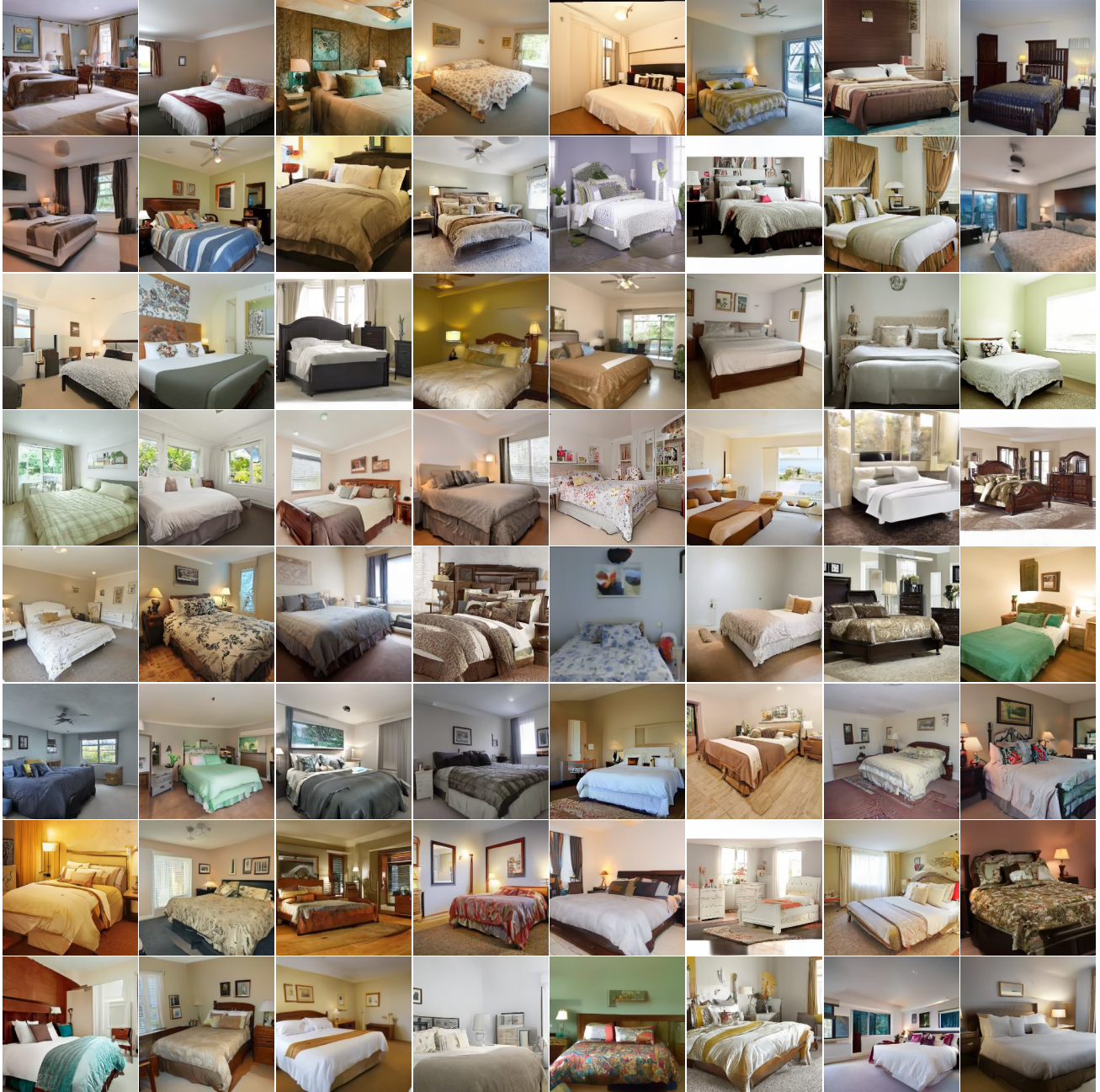


Figure 13: Additional qualitative results on LSUN-Bedroom (256×256).



Figure 14: Additional qualitative results on LSUN-Church (256×256).



Figure 15: Additional qualitative results on FFHQ (256×256).



Figure 16: Additional qualitative results on high resolution FFHQ dataset (1024×1024).